Scattering of obliquely incident electromagnetic plane waves by composite panels involving periodic arrays of circular fibers

C.Y. Li[*1], *D. Lesselier*[1], *and Y. Zhong*[2]

[1]Département de Recherche en Electromagnétisme-Laboratoire des Signaux et Systèmes
UMR8506 (CNRS-SUPELEC-Univ Paris-Sud), *changyou.li@lss.supelec.fr, lesselier@lss.supelec.fr*

[2]A*STAR, Institution of High Performance Computing, 138632 Singapore, *zhongyu@ihpc.a-star.edu.sg*

Abstract

The electromagnetic behavior of a single-layer slab comprising a periodic array of infinite circular cylindrical fibers is considered for a plane wave illumination whose wave vector is orientated obliquely vs. the fibers' axes. Full-wave field representations in this 2.5-D scattering case from multipole and plane-wave expansions are used for calculating reflection and transmission coefficients of the longitudinal field components by matching the modes at the boundaries. Power reflection and transmission coefficients are obtained from time-averaged Poynting vectors.To model a multi-layered structure made by stacking periodic slabs one over the other is the next extension. Among applications, non-destructive testing of a disorganized structure comes to the fore, as well as the making of frequency and polarization selective devices.

1. Introduction

The time-harmonic electromagnetic response of multi-layer fiber-reinforced composites is considered. For each layer, the composite consists of a periodic arrangement of infinite cylindrical circular fibers (reinforcements) embedded inside a given background material (matrix), all the fibers being oriented into the same direction. Multi-layer composites are constructed by stacking up single-layer structures one over the other, the orientations in different layers possibly differing from another. (This is a small-scale view, refer to [1] for a large-scale view wherein homogeneization of any given layer leads to uniaxial aniostropic permittivities.)

Herein, one investigates the single-layer composite structure for 3D incident plane waves (2.5D case), which means their wave vector is not orthogonal to the fibers' axes (or equivalently does not lie inside the cross-sectional plane of the fibers). To characterize multi-layer composites, matching the modes at the boundaries between different layers then suffices, which is under investigation at the time of writing.

To obtain the power reflection and transmission coefficients in this 2.5-D scattering case, the longitudinal components of the fields are firstly expanded with multipole and plane-wave expansions. Accounting for the relationship between the transverse and longitudinal components of the fields, the plane-wave expansion coefficients are expressed in terms of multipole expansion coefficients by matching the modes at the boundaries. The multipole expansion coefficients are then obtained through establishing the Rayleigh's identity. Power reflection and transmission coefficients are easily obtained with the time-averaged Poynting vectors.

As far as one knows, the present approach for the scattering of 3D incident waves by such a 2D periodic structure is firstly proposed in this paper. It is based on the previous work for the 2D case of TE/TM polarized incident waves [2] which borrows in a good part from the earlier poro-acoustics and elasticity analyses [3] and photonic ones [4].

2. Configuration and methodology

The structure is sketched in Fig. 1(a). The cylinders, periodically embedded in the slab along the x direction, are parallel to one another, their axes being orientated towards the y direction, letting center-to center distance d and radius c. The structure, with upper and lower boundaries Γ_a ($z = a$) and Γ_b ($z = b$), divides the space into four regions, R_0, R_1, R_2 and R_3. Materials in them are possibly different from one another but all are isotropic. ϵ_j, ϵ_{rj}, μ_j, and μ_{rj}, $j = 0, 1, 2, 3$, are their permittivities, relative permittivities, permeabilities and relative permeabilities in corresponding regions.

One assumes that the wave vector of the incident wave is $\vec{k}^i = k^i_x\hat{x}+k^i_y\hat{y}-k^i_z\hat{z}$, and the angle between the z-axis and $\vec{k}^i$ is ϑ, and the one between the x-axis and the projection of $\vec{k}_i$ in the x-y plane is φ, as shown in Fig. 1(b). $\hat{x}$, $\hat{y}$ and $\hat{z}$ are the unit vectors in the x, y and z directions. Hence, $k^i_x = -k^i \sin\vartheta\cos\varphi$, $k^i_y = k^i \sin\vartheta\sin\varphi$ and $k^i_z = k^i\cos\vartheta$. $\vec{k}^i_t$ is the transverse component of $\vec{k}^i$, which lies within the x-z plane. The angle between $\vec{k}^i_t$ and the z axis is θ_i. Defining the wave vectors in different regions and their transverse components as $\vec{k}_j$ and $\vec{k}_{tj}$, thus, $k^2_{tj} = k^2_j - k^2_{yj}$ and $\vec{k}_{tj} = k_{xj}\hat{x}-k_{zj}\hat{z}$. Here, one sets $\vec{k}_{tj} = \hat{x}\alpha_j - \hat{z}\beta_j$, and $\alpha_j = k_{xj}$ and $\beta_j = k_{zj}$. The incident wave is described as $\boldsymbol{\mathcal{E}}(x, y, z) = \boldsymbol{\mathcal{E}}^{inc}e^{i(k^i_x x+k^i_y y-k^i_z z)}$

978-1-4673-5225-3/14/$31.00 ©2014 IEEE

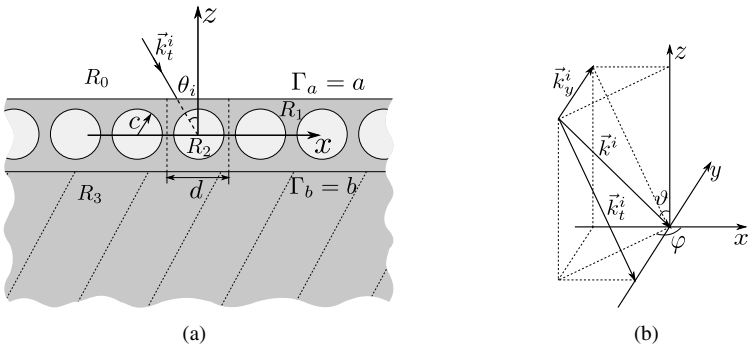

Fig. 1: (a) A slab including a periodic set of cylindrical fibers with the transverse components of incident plane wave; (b) The relations between the wave vector $\vec{k}^i$ of obliquely incident electromagnetic plane wave and its components $\vec{k}_y^i$, $\vec{k}_t^i$.

and $\boldsymbol{\mathcal{H}}(x,y,z) = \boldsymbol{\mathcal{H}}^{inc} e^{i(k_x^i x + k_y^i y - k_z^i z)}$ with implicit time-dependence $e^{-i\omega t}$. $\boldsymbol{\mathcal{E}}^{inc} = E_x^i \hat{x} + E_y^i \hat{y} + E_z^i \hat{z}$ and $\boldsymbol{\mathcal{H}}^{inc} = H_x^i \hat{x} + H_y^i \hat{y} + H_z^i \hat{z}$ are all constant vectors.

The key feature of the problem is the transverse periodicity of the inclusions. According to the Floquet theorem, this periodicity and the plane wave nature of the field lead to the Floquet relation $\mathbf{V}_j(x+d,z) = \mathbf{V}_j(x,z)e^{i\alpha_0 nd}$.

For propagating fields in all regions, each mode is characterized by its propagation constant k_{jy} in the y direction and its transverse dependence of the fields lying in the x-z plane, which means $\boldsymbol{\mathcal{E}}_j(x,y,z) = \mathbf{E}_j(x,z)e^{ik_{jy}y}$ and $\boldsymbol{\mathcal{H}}_j(x,y,z) = \mathbf{K}_j(x,z)e^{ik_{jy}y}$ with $\mathbf{E}_j(x,z)$ encompassing the transverse dependence of the electric field and $\mathbf{K}_j(x,z) = \sqrt{\mu_0/\epsilon_0}\mathbf{H}_j(x,z)$ the one of the scaled magnetic field. Each such field satisfies the Helmholtz equation $(\nabla^2 + k_{tj}^2)\mathbf{V}_j = 0$, where $\mathbf{V}_j$ denotes either $\mathbf{E}_j$ or $\mathbf{K}_j$. Each component of $\mathbf{V}_j$ must be continuous across the interfaces Γ_a and Γ_b.

Noticing that $\mathbf{V} = (\mathbf{V}_t + V_y\hat{y})$ and $\mathbf{V}_t = V_x\hat{x} + V_z\hat{z}$, one decomposes its divergence as $\nabla \cdot \mathbf{V} = \nabla_t \cdot \mathbf{V}_t + ik_y V_y$ and its curl as $\nabla \times \mathbf{V} = \nabla_t \times \mathbf{V}_t + ik_y\hat{y} \times \mathbf{V}_t - \hat{y} \times \nabla_t V_y$, where ∇_t is $\frac{\partial}{\partial x}\hat{x} + \frac{\partial}{\partial z}\hat{z}$ in the Cartesian coordinate system and $\frac{\partial}{\partial r}\hat{r} + \frac{1}{r}\frac{\partial}{\partial \theta}\hat{\theta}$ in the polar coordinate system. The index j is neglected here for convenience since the equations hold in all regions. Decomposing the field $\boldsymbol{\mathcal{E}}$ and $\boldsymbol{\mathcal{H}}$ into longitudinal and transverse components, parallel to and orthogonal with the cylinder axes, respectively, denoted by subscripts y and t, one has $\boldsymbol{\mathcal{E}} = (\mathbf{E}_t + E_y\hat{y})e^{ik_{jy}y}$, $\boldsymbol{\mathcal{H}} = (\mathbf{H}_t + H_y\hat{y})e^{ik_{jy}y}$. Letting k as propagation constant in air, the transverse fields are given in terms of longitudinal ones as [5,6]

$$\mathbf{E}_t = i/k_t^2[k_y\nabla_t E_y - \sqrt{\mu_0/\epsilon_0}k\mu_r\hat{y} \times \nabla_t H_y], \tag{1a}$$

$$\mathbf{H}_t = i/k_t^2[k_y\nabla_t H_y + \sqrt{\epsilon_0/\mu_0}k\epsilon_r\hat{y} \times \nabla_t E_y], \tag{1b}$$

Considering the longitudinal fields, their representations in regions R_0 and R_3 read as

$$E_{0y}(x,z) = \sum_{p\in\mathbb{Z}}(E_y^i e^{-i\beta_{0p}(z-a)}\delta_{p0} + R_p^e e^{i\beta_{0p}(z-a)})e^{i\alpha_p x}, \tag{2a}$$

$$K_{0y}(x,z) = \sum_{p\in\mathbb{Z}}(K_y^i e^{-i\beta_{0p}(z-a)}\delta_{p0} + R_p^h e^{i\beta_{0p}(z-a)})e^{i\alpha_p x}, \tag{2b}$$

$$E_{3y}(x,z) = \sum_{p\in\mathbb{Z}} T_p^e e^{i(\alpha_p x - \beta_{3p}(z-b))}, \tag{2c}$$

$$K_{3y}(x,z) = \sum_{p\in\mathbb{Z}} T_p^h e^{i(\alpha_p x - \beta_{3p}(z-b))}. \tag{2d}$$

$R_p^{e,h}$ and $T_p^{e,h}$ are the reflection and transmission coefficients of the plane wave indexed by p, δ_{p0} the Kronecker symbol, $\alpha_p = \alpha_0 + 2p\pi/d$, $\beta_{jp} = \sqrt{k_{tj}^2 - \alpha_p^2}$. Because of the continuity of α_{jp} across Γ_a and Γ_b, α_p is used everywhere instead. For R_1, the field representations are obtained by applying the Green's second identity around the boundary of one primary cell with the periodic Green's function $G(\mathbf{r}) = -\frac{i}{4}\sum_{n=-\infty}^{+\infty} e^{i\alpha_0 nd}\mathrm{H}_0^{(1)}(k_{1t}|\mathbf{r} - nd\hat{x}|)$, where $\mathrm{H}_0^{(1)}$ is the 1st-kind Hankel function of 0-th order. The field representations are written as

$$E_{1y}^{\pm}(x,z) = \sum_{p\in\mathbb{Z}}(f_{ep}^- e^{-i\beta_{1p}z} + f_{ep}^+ e^{i\beta_{1p}z})e^{i\alpha_p x} + \sum_{p\in\mathbb{Z}}\sum_{m\in\mathbb{Z}} B_m^e Q_{pm}^{\pm} e^{i(\alpha_p x \pm \beta_{1p}z)}, \tag{3a}$$

$$K_{1y}^{\pm}(x,z) = \sum_{p\in\mathbb{Z}}(f_{hp}^- e^{-i\beta_{1p}z} + f_{hp}^+ e^{i\beta_{1p}z})e^{i\alpha_p x} + \sum_{p\in\mathbb{Z}}\sum_{m\in\mathbb{Z}} B_m^h Q_{pm}^{\pm} e^{i(\alpha_p x \pm \beta_{1p}z)}, \tag{3b}$$

where $f_{ep}^{\pm}$ and $f_{hp}^{\pm}$ account for the field scattered by the plate, the signs $+$ and $-$ corresponding to $z > c$ and $z < -c$. B_m^e

and B_m^h are the multipole expansion coefficients, $Q_{pm}^{\pm} = \frac{2(-i)^m}{d\beta_{1p}} e^{\pm im\theta_p}$ [3, 7, 8]. The forms of the transverse fields E_x, E_z, K_x and K_z in both Cartesian and cylindrical coordinates easily follow. Matching the modes at both Γ_a and Γ_b, the coefficients R_p^e, R_p^h, T_p^e, T_p^h, f_{ep}^+, f_{ep}^-, f_{hp}^+ and f_{hp}^- are all expressed with B_m^e and B_m^h obtained by solving the Rayleigh's identity established by matching the boundary conditions around the fibers [6]. All lengthy expressions are omitted here.

From time-averaged Poynting vectors, the power reflection and transmission coefficients are defined as $\boldsymbol{\mathcal{R}} = \sum_{p\in\mathbb{Z}} \mathcal{R}_p$, $\boldsymbol{\mathcal{T}} = \sum_{p\in\mathbb{Z}} \mathcal{T}_p$ and $\boldsymbol{\mathcal{A}} = 1 - \boldsymbol{\mathcal{R}} - \boldsymbol{\mathcal{T}}$ with $\mathcal{R}_p = \Re\{(R_p^e \xi_p^{r*} - R_p^{h^*} \zeta_p^r)/(K_{inc}^* \xi_p^i - E_{inc} \zeta_p^{i^*})\}$ and $\mathcal{T}_p = \Re\{(T_p^{h*} \xi_p^t - T_p^e \zeta_p^{t^*})/(K_{inc}^* \xi_p^i - E_{inc} \zeta_p^{i^*})\}$, where the coefficients are

$$\xi_p^i = \frac{k_y \alpha_0 E_{inc} + k\mu_{0r}\beta_0 K_{inc}}{k_{0t}^2}, \quad \zeta_p^i = \frac{k_y \alpha_0 K_{inc} - k\epsilon_{0r}\beta_0 E_{inc}}{k_{0t}^2}, \quad \xi_p^r = \frac{k_y \alpha_p R_p^h + k\epsilon_{0r}\beta_{0p} R_p^e}{k_{0t}^2},$$
$$\zeta_p^r = \frac{k_y \alpha_p R_p^e - k\mu_{0r}\beta_{0p} R_p^h}{k_{0t}^2}, \quad \xi_p^t = \frac{k_y \alpha_p T_p^e + k\mu_{3r}\beta_{3p} T_p^h}{k_{3t}^2}, \quad \zeta_p^t = \frac{k_y \alpha_p T_p^h - k\epsilon_{3r}\beta_{3p} T_p^e}{k_{3t}^2}.$$

3. Lattice sums

Dealing with lattice sums is one of the difficulties for calculating electromagnetic wave scattering by periodic structures. For the 1D periodicity, they are defined as $S_m = \sum_{n=1}^{\infty} \mathrm{H}_m^{(1)}(k_{t1}nd)[e^{i\alpha_0 nd} + (-1)^m e^{-i\alpha_0 nd}]$ with $\mathrm{H}_m^{(1)}(x)$ the 1st-kind Hankel function of m-th order. It can not be calculated directly because of the slow convergence. Much literature exists for accelerating it [9–13]. Here, one of the most recent methods [13] is used, referring to [2] for numerical examples.

4. Numerical results

Defining the relative error $|\boldsymbol{\mathcal{R}}^{n+1} - \boldsymbol{\mathcal{R}}^n|$, $n = P, M$, the infinite sums $\sum_{p\in\mathbb{Z}}$ and $\sum_{m\in\mathbb{Z}}$ are truncated as $\sum_{p=-P}^{P}$ and $\sum_{m=-M}^{M}$ with $P = \mathrm{Int}\,(d/2\pi(3\Re(k_1) - \alpha_0))$, $M = \mathrm{Int}\,\big(\Re(4.05 \times (k_1 c)^{1/3}) + k_1 c\big)$ [3] to achieve an approximation with relative error less than 10^{-6}, refer to [2] for details.

To verify the approach, the power reflection coefficients of the 0-th mode for normal incidence of TM/TE wave impinging on carbon ($\epsilon_{r2} = 12$, $\sigma = 3.3 \times 10^2\,\mathrm{S\,m^{-1}}$) fiber-reinforced composites (CFRC) are obtained by setting $E_y^i = 1$, $K_y^i = 0$ and $E_y^i = 0$, $K_y^i = 1$ respectively. Epoxy ($\epsilon_{r1} = 3.6$), as widely used background material, is chosen for the slab. The wavelength of the incident wave is $\lambda_i = 0.1$ mm, and $\varphi = 0$. The size of the structure is set to $d = L = \lambda_i$, $c = 0.25d$, which is used in the whole paper. As shown in Fig. 2, the results match well with those from COMSOL FEM code.

The results of $\boldsymbol{\mathcal{R}}$ for glass ($\epsilon_{r2} = 6$) fiber-reinforced composites (GFRC) are given in Fig. 3 with $L = d = \lambda_i = 0.1mm$; several peaks appear when ϑ varies from $-90°$ to $90°$ and good symmetry is observed. When $\varphi = 45°$, the reflection is stronger than that of $\varphi = 90°$ except ϑ close to 0 (normal incidence).

The variation of $\boldsymbol{\mathcal{R}}$ with d/λ_0 for GFRC is given in Fig. 4 for different values of φ with $\vartheta = 60°$, which is the essential situation for periodic structures used as frequency and polarization selective components in microwave and optical regions. Several narrow peaks are observed, some associated to full reflection phenomenon, all (if one zooms onto them via small steps of d/λ_0) vary quite smooth however. Though investigation is still pending, they should be closely related to modified plate modes arising from complex interference between the plate and the array embedded in it. $\boldsymbol{\mathcal{R}}$ approaches to zero when d/λ_0 is small, hence, for Non-destructive Testing (NdT) of GFRC, the frequency is chosen from 10 GHz to 60 GHz. For CFRC, results for $\boldsymbol{\mathcal{R}}$ and $\boldsymbol{\mathcal{T}}$ varying with d/λ_0 are in Fig. 5, where $\vartheta = 60°$. Strong absorption is observed when d/λ_0 approaches 1, but, for the long wavelength case, strong transmission is obtained. For the general NdT frequency band from 1 MHz to 1 GHz, $\boldsymbol{\mathcal{R}}$ for $\varphi = 45°$ and $\varphi = 90°$ are about 0.2 and 0.1.

5. Conclusion

Scattering from a single-layer of slab involving a periodic array of circular cylinders has been investigated for 3D plane wave illumination. The method, firstly proposed here, is intrinsically frequency-broad-band and valid for any isotropic constitutive material. Its effectiveness and accuracy are illustrated from numerical results for single-layer carbon/glass fiber-reinforced composites as in aeronautic and automotive parts. Applying the approach to analyze the electromagnetic characterization of multi-layer periodic slab is under investigation.

The present work and forthcoming contributions are also essential if one wishes to image a disorganized periodic structure (caused by taking away/displacing cylinders, or changing electromagnetic properties or shapes of cylinders in the layers). A good understanding of the behavior of both periodic and disorganized periodic structures is indeed needed, the dyadic Green's functions following from plane-wave expansions of the fields due to inner or outer elementary dipoles.

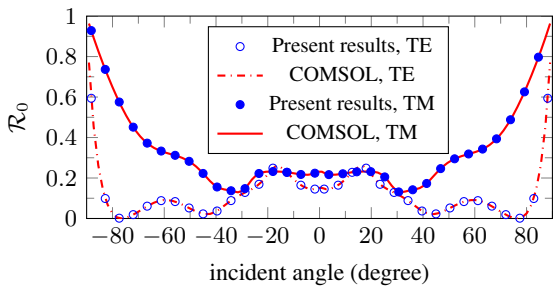

Fig. 2: TE and TM case validation with $d = \lambda_i = 0.1$ mm, $L = d$ and $c = 0.25d$.

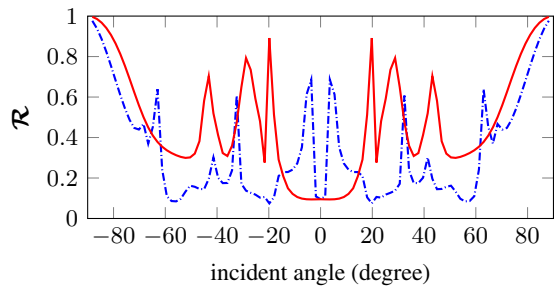

Fig. 3: Variation of $\mathcal{R}$ with ϑ for $\varphi = 45°$ (dash-dotted line) and $\varphi = 90°$ (solid line), glass fibers

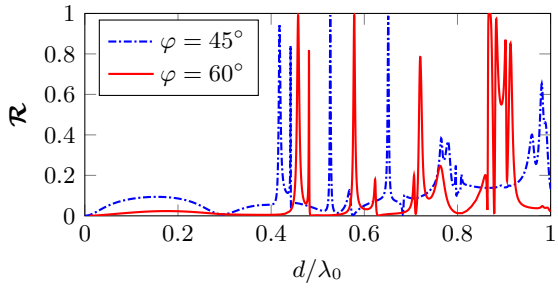

Fig. 4: Variation of $\mathcal{R}$ with d/λ_0, glass fibers, $L = d = 0.1mm$, $c = 0.25d$, $\vartheta = 60°$

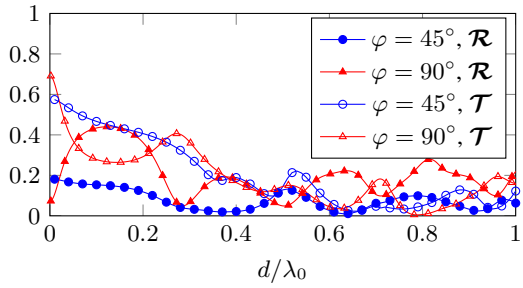

Fig. 5: Variation of $\mathcal{R}$ and $\mathcal{T}$ with d/λ_0 for $\varphi = 45°$ and $\varphi = 90°$, carbon fibers

6. References

1. Y. Zhong, M. Lambert, D. Lesselier and X. Chen, "Electromagnetic response of anisotropic laminates to distributed sources", *IEEE Trans. Antennas Propagat.*, **62**, 247-256, 2014

2. C.Y. Li, D. Lesselier, and Y. Zhong, "Electromagnetic small-scale modeling of composite panels involving periodic arrays of circular fibers", *5th International Conference on Metamaterials, Photonic Crystals and Plasmonics*, Singapore, 2014

3. J.-P. Groby, A. Wirgin, L. D. Ryck, W. Lauriks, R. P. Gilbert, and Y. S. Xu, "Acoustic response of a rigid-frame porous medium plate with a periodic set of inclusions", *J. Acoust. Soc. Am.*, **126**, 685-693, 2009

4. J.-P. Groby and D. Lesselier, "Localization and characterization of simple defects in finite-size photonic crystals", *J. Optical Soc. Am. A*, **25**, 146-152, 2008

5. A. Snyder and J. Love, *Optical Waveguide Theory, Part III*, London, Chapman and Hall, 1996

6. S. Guenneau, C. Poulton, and A. Movchan, "Oblique propagation of electromagnetic and elastic waves for an array of cylindrical fibers", *Proc. Royal Soc. A.*, **459**, 2215-2263, 2003

7. S. Wilcox, L. C. Botten, R. C. McPhedran, C. G. Poulton, and C. Martijn de Sterke, "Modeling of defect modes in photonic crystals using the fictitious source superposition method", *Phys. Rev. E*, **71**, 056606-1-056606-11, 2005

8. L. C. Botten, "Formulation for electromagnetic scattering and propagation through grating stacks of metallic and dielectric cylinders for photonic crystal calculations. Part I. Method", *J. Opt. Soc. Am. A*, **17**, 2165-2176, 2000

9. V. Twersky, "On scattering of waves by the infinite grating of circular cylinders", *IEEE Trans. Antennas Propagat.*, **10**, 737-765, 1962

10. K. Yasumoto and K. Yoshitomi, "Efficient calculation of lattice sums for free-space periodic Green's function", *IEEE Trans. Antennas Propagat.*, **47**, 1050-1055, 1999

11. A. Moroz, "Exponentially convergent lattice sums", *Opt. Lett.*, **26**, 1119-1121, 2001

12. M. Kavaklioglu, "On Schlömilch series representation for the transverse electric multiple scattering by an infinite grating of insulating dielectric circular cylinders at oblique incidence", *J. Phys. A: Math. Gen.*, **35**, 2229-2234, 2002

13. C. M. Linton, "Schlömilch series that arise in diffraction theory and their efficient computation", *J. Phys. A: Math. Gen.*, **39**, 3325-3339, 2006